J. Fluid Mech. (1994), vol. 262, pp. 353–375

A bifurcation study of viscous flow through a rotating curved duct

By M. SELMI[1], K. NANDAKUMAR[2] AND W. H. FINLAY[3]

[1]Mechanical Engineering Department, Qatar University, PO Box 2713, Doha - Qatar

[2]Department of Chemical Engineering, University of Alberta, Edmonton, Alberta, Canada, T6G 2G6

[3]Department of Mechanical Engineering, University of Alberta, Edmonton, Alberta, Canada, T6G 2G8

(Received 18 May 1993 and in revised form 15 September 1993)

The combined effects of system rotation (Coriolis force) and curvature (centrifugal force) on the bifurcation structure of two-dimensional flows in a toroidal geometry of rectangular cross-section are examined. The problem depends on the Rossby number, $Ro = U/b\Omega$, the Ekman number, $Ek = \nu/b^2\Omega$, the aspect ratio, $\gamma = b/h$ and the radius ratio, $\eta = r_i/r_o$; here U is the velocity scale, b is the channel width in the spanwise direction, Ω is the rotational speed, (r_i, r_o) are the inner and outer radii of the duct, $h = r_o - r_i$ is the channel gap in the radial direction and ν is the kinematic viscosity of the fluid. A pseudospectral method is devised to discretize the two-dimensional Navier–Stokes equation in stream-function form. Continuation schemes are used to track the solution paths with Rossby number as the control parameter. Extended systems are used to determine the precise location of the singular points of the discretized system. The loci of such singular points are tracked with respect to curvature of the duct. Unlike the findings of Miyazaki (1973) on the same problem, curvature is found to have profound effects on the solution structure; flow mutations take place through a tilted cusp at ($Ro = 7.122, \eta = 0.678$) and a transcritical bifurcation point at ($Ro = 1.357, \eta = 0.349$).

1. Introduction

1.1. *Curved ducts*

Pressure-driven flow through curved pipes has drawn sustained attention since the early experimental works of Eustice (1910, 1911). Dean (1927) was the first to formulate the problem in mathematical terms under the fully developed (or axially invariant, two-dimensional) flow conditions. He demonstrated the existence of a pair of counter-rotating vortices as a secondary flow superimposed on the primary Poiseuille flow in a curved pipe. Hence it has come to be known as the *Dean problem.* Since Dean's original analysis, a vast literature has evolved on this problem and is reviewed by Berger, Talbot & Yao (1983) and Nandakumar & Masliyah (1986). For our purposes, relevant work on the Dean problem is focused on *centrifugal instability* and the bifurcation of two-dimensional solutions with increasing Dean numbers. Cheng & Akiyama (1970) were the first to mention dual solutions in loosely coiled curved ducts. Since then multiple solutions for fully developed flow in a curved duct of square cross-section have been found in the numerical studies of Winters &

Brindley (1984), Shanthini & Nandakumar (1986), Winters (1987), Daskopoulos & Lenhoff (1989) and Bara, Nandakumar & Masliyah (1992).

Winters (1987) has presented the most comprehensive bifurcation study on the Dean problem, documenting the multiple solution structure consisting of both symmetric and asymmetric solutions. A linear stability analysis by Winters revealed that the two-vortex solutions on the primary branch are stable to any arbitrary two-dimensional perturbation, while the four-vortex solutions are conditionally stable to symmetric perturbations but unstable to asymmetric perturbations. Despite the predicted instability of four-vortex flows, they have been visualized by Cheng, Nakayama & Akiyama (1979) and Sugiyama, Hayashi & Yamazaki (1983) at certain Dean numbers in their experiments, but not as dual solutions (i.e. co-existing at the same Dean number as a two-vortex flow). In a recent study Bara *et al.* (1992) have experimentally examined the development of multiple two-dimensional solutions from well-prescribed inlet conditions in curved ducts of square cross-section using laser Doppler anemometry and verified many of Winter's predictions.

1.2. *Rotating ducts*

The pressure-driven viscous flow through straight pipes can also exhibit a complex secondary flow structure when the pipe is rotated about an axis perpendicular to its own. In this case the secondary flow pattern is generated and sustained by the *Coriolis force* introduced by the duct rotation. Interest in Coriolis-force-driven secondary flows stems in part from their presence in rotating machinery (Walker 1975) and in instruments that measure mass flow rates based on the Coriolis effect (Raszillier & Durst 1991; Durst & Raszillier 1990). As with the Dean problem, our interest in the rotating duct is with the stability aspects of the flow. This aspect has been investigated by numerous investigators in the idealized infinite geometry (Hart 1971; Lezius & Johnston 1976; Alfredsson & Persson 1989; Finlay 1990, 1992) as well as in more practical finite geometries of square (Kheshgi & Scriven 1985; Nandakumar *et al.* 1991), rectangular (Speziale 1982; Speziale & Thangam 1983) and circular (Barua 1954; Mansour 1985; Duck 1983) cross-sections. Typically, two parameters govern the dynamics of flow in rotating channels. They are (i) the Ekman number, defined as $Ek = \nu/b^2\Omega$, which represents the ratio of viscous to Coriolis force, and (ii) the Rossby number, defined as $Ro = U/b\Omega$, which represents the ratio of the convective acceleration to the Coriolis force. Here Ω is the magnitude of the angular velocity, b is the length-scale representing the channel width (figure 1), ν is the kinematic viscosity and U is the axial velocity scale which is taken to be $U = -(1/\rho\Omega b)(\partial\varphi/\partial\phi)$ where φ is a potential that combines the centrifugal, gravitational and thermodynamic pressure terms and ϕ is the angle measured in the streamwise direction; ρ is the density of the fluid.

The solution to the rotating duct problem is obtainable by analytical means in the asymptotic limits of slow and rapid rotation and the flow structure is well understood for these cases. When the three forces (convective acceleration, viscous and Coriolis forces) are of comparable magnitude, however, nonlinear effects can be quite strong and the flow structure can be unraveled only through numerical means. Recognizing this, Duck (1983) has used a numerical procedure, based on a combination of Fourier decomposition and finite difference discretization to study the flow structure in rotating circular ducts. However, owing to convergence difficulties of the iterative solution method used, no solutions at high Rossby numbers could be obtained. In particular a dual four-vortex solution was not computed. Solution multiplicity is, however, expected since the equations governing the two-dimensional flows through

rotating channels are analogous to those of laminar flow in coiled ducts (the Dean problem) in the double limit of $Ek \to \infty$, $(Ro/Ek) \to \infty$, and $(Ro/Ek^2) =$ constant as shown for example by Mansour (1985). In a numerical study of the flow in a rotating, rectangular duct Speziale (1982, 1983) demonstrated that a transition from a two-cell to a four-cell structure occurs as the Rossby number is changed. The tasks of demonstrating that both flow structures are possible over a range of Rossby numbers and that an intermediate branch connecting the two- and four-cell solution branches exists were accomplished by Kheshgi & Scriven (1985) who used a finite element discretization and Euler–Newton continuation. For the case of $Ek = 0.01$, they detected and bracketed the values of two limit points. Furthermore, they tracked the variation of one of the limit points with Ekman number. However, they did not use the extended system formulation to compute the limit points precisely or track their variation with other parameters. Also, reflection symmetry in the problem was exploited to reduce the computational domain by half. Hence no asymmetric solutions could be detected in their simulations. In a more recent work Nandakumar *et al.* (1991) constructed the complete bifurcation diagram for the rotating duct problem along the lines of Winters' contribution to the Dean problem.

1.3. *Common features of the flow*

Several features of the solution structure found by Winters for the Dean problem are similar to those presented by Nandakumar *et al.* (1991) for rotating rectangular ducts and also those occurring in non-isothermal mixed-convection heat transfer in a square duct (Nandakumar & Weinitschke 1991), also known as the *Morton problem*, where buoyancy-induced instability causes similar structural changes in the solution.

All of these three problems (the Dean problem, rotating duct problem and the Morton problem) discussed above share the following common features:

(i) The primary flow in the streamwise direction is pressure driven in a finite-geometry duct or tube with an inlet and outlet. Thus the flow is inherently three-dimensional near the inlet region. In certain regions of the parameter space, the flow develops from the inlet condition and reaches a streamwise-invariant state for low values of the dynamical parameter.

(ii) A secondary flow is generated by a body force (centrifugal, Coriolis or buoyancy force) and this secondary flow is always present for any non-zero forcing of the body force. As a consequence, the flow is always at least two-dimensional in nature. Often a three-dimensional inlet region of sufficient length is needed for the flow to develop into an invariant state in the streamwise direction.

(iii) The primary flow pattern breaks down above a critical value of the forcing parameter (Dean number, Rossby number or Grashof number) leading to a complex bifurcation structure involving two-dimensional flows.

(iv) Of the several co-existing two-dimensional flow structures (i.e. multiple solutions) one that warrants some scrutiny is a four-cell secondary flow structure which is predicted to be conditionally stable in all of the three problems. In particular this four-cell flow is unstable to asymmetric perturbations. Yet, it remains observable in experiments on the Dean problem. This is believed to be due to the slow growth rates of the unstable asymmetric modes.

(v) There is a range of the forcing parameter wherein no stable two-dimensional solutions are present. In this region some form of fully developed three-dimensional flow must evolve. Computations and experiments with the Dean problem indicate that a streamwise-periodic three-dimensional flow evolves first, followed by the formation

of travelling waves. Such phenomena in the other two problems have not yet been explored.

The development of two-dimensional solutions from a given inlet profile in curved ducts of rectangular cross-section has been studied by numerous investigators (Ghia & Sokhey 1977; Humphrey, Taylor & Whitelaw 1977; Yee, Chilukuri & Humphrey 1980; Taylor, Whitelaw & Yianneskis 1982; Hille, Vehrenkamp & Schulz-Dubois 1985; Sankar, Nandakumar, & Masliyah 1988; Soh 1988). The most detailed measurements of the flow development in a curved duct of square cross-section were performed using laser Doppler anemometry by Hille *et al.* (1985) and by Bara *et al.* (1992). The measurements of Hille *et al.* (1985) revealed the development of an asymmetric four-vortex structure at Dean numbers between 150 and 300, but the flow had not reached a fully developed state within the 180° axial length of their duct. In the numerical study of the flow development in a curved duct of square cross-section, Sankar *et al.* (1988) found that it was possible for a four-vortex flow to develop sustained spatial oscillations in the streamwise direction. The numerical study by Soh (1988) showed that, depending on the inlet condition for a given flow rate, the flow might develop into the two-cell and four-cell states predicted by the two-dimensional bifurcation study of Winters (1987).

1.4. *Combined effects of curvature and system rotation*

As a natural extension to this class of problems, the effect of *system rotation* on curved duct flow has been investigated by numerous investigators. Ludwieg (1951) and Hocking (1967) developed a solution based on the momentum integral method. Miyazaki (1971, 1973) examined the solution when the pressure-driven flow and the sense of rotation are in the same direction. In such cases the flow resistance was found to increase with the strength of rotation. Itō & Motai (1974) examined both co- and counter-rotating cases with respect to the direction of pressure-driven flow. With the counter-rotating case, a reduction in the strength of the secondary flow and even a secondary flow reversal was observed. Experiments on rotating curved ducts have been performed by Piesche & Felsh (1980). In the most recent study on this problem, Daskopoulos & Lenhoff (1990) have presented the first and most comprehensive bifurcation study of this combined problem. Note that Daskopoulos & Lenhoff (1990) have considered a circular geometry, with a symmetry condition imposed along the centreline. Thus questions concerning non-symmetric solutions and symmetry-breaking bifurcations have been left unanswered. They have also invoked the loose-coiling approximation.

Even for the pure Dean problem without system rotation, the solution structure for the circular cross-section is still not fully understood. For example it is not clear whether symmetry-breaking bifurcation can occur in such geometries. There is also the long-standing controversy regarding the asymptotic behaviour of the friction factor *vs.* Dean number relationship (Van Dyke 1978; Dennis 1980; Ramshankar & Sreenivasan 1988; Dennis & Riley 1982). On the other hand, the bifurcation structure in curved ducts (Winters 1987) and rotating straight ducts (Nandakumar *et al.* 1991) of square cross-section is well understood. Hence a square cross-section is appropriate for a comprehensive study when both curvature and system rotation are present and this is the focus of our present study.

Neither the loose-coiling approximation nor symmetry conditions are imposed in our study. The nonlinear equations are discretized using a pseudospectral discretization with Chebyshev polynomials. We construct the bifurcation diagrams using Rossby number as the control parameter. The Eckman number is fixed at $Ek = 0.01$

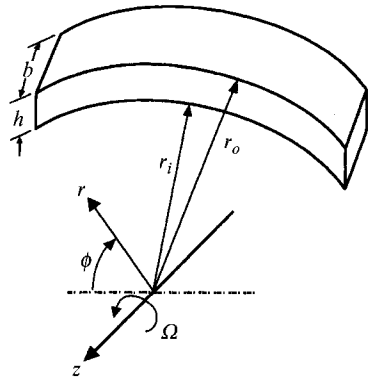

FIGURE 1. Description of a toroidal geometry of rectangular cross-section in cylindrical coordinate system.

and a square cross-section is considered. The primary solution branch that originates at $Ro = 0$ is tracked as a function of Rossby number for both counter-clockwise and clockwise rotation of the duct. In addition, isolated symmetric solution branches and asymmetric branches which emanate from symmetry-breaking bifurcation points are discovered for each case. The effect of curvature on the structural changes to the solution are examined at three different curvature ratios. The location of the limit points and symmetry-breaking bifurcation points are determined precisely using the extended system formulations (Moore & Spence 1980; Spence & Werner 1982; Werner & Spence 1984). The loci of these singular points as the curvature is varied are computed using a fold-following scheme. Linear stability is determined by computing the complete spectrum of eigenvalues of the discretized problem at selected Rossby numbers on all of the solution branches. As there is no method of predicting *a priori* the total number of solutions for a given parameter set, one still cannot be certain that all the solution branches of interest have been discovered. However, a self-consistent picture of the solution structure emerges from the study. Several new features of the solution structure are revealed that are not present in the Dean problem.

2. Governing equations

We consider the flow of an incompressible fluid of density ρ and viscosity μ through a curved duct of width b in the spanwise direction, height h in the radial direction, and rotating about its axis of curvature at the rate Ω (see figure 1). Note that the geometry is toroidal and hence finite pitch effects are not considered. The rotation can be co-rotational, in which case velocities associated with the angular rotation Ω are in the same direction as the pressure-driven streamwise flow, or counter-rotational, where the channel walls rotate in the opposite direction to the primary pressure gradient. The inner and outer walls of the duct have radii of curvature r_i and r_o respectively as shown in figure 1. We use cylindrical coordinates (ϕ, r, z), where ϕ, r, z are the streamwise, normal, and spanwise directions respectively with the axis of curvature defined as $r = 0$ and the middle of the duct in the spanwise direction defined as $z = 0$. The flow is driven by a mean pressure gradient $\partial\bar{p}/\partial\phi$ in the streamwise direction.

The Navier–Stokes equations governing the two-dimensional flow through the duct are non-dimensionalized using b to scale length in the z-direction, h to scale length in the radial direction, $U = -(1/\rho\Omega b)\partial\varphi/\partial\phi$ to scale velocities, where φ is a potential

that combines pressure, gravitational, and centrifugal forces, $\rho U b\Omega$ to scale pressure, and $1/\Omega$ to scale time. If the velocity is expressed in terms of cylindrical components (u_ϕ, u_r, u_z), these equations take the form

$$\mathrm{D}u_\phi + Ro\frac{\gamma}{r}u_r u_\phi - 2\epsilon u_r = \frac{\gamma}{r} + Ek\left[\nabla^2 u_\phi - \frac{\gamma^2}{r^2}u_\phi\right], \tag{2.1}$$

$$\mathrm{D}u_r - Ro\frac{\gamma}{r}u_\phi^2 + 2\epsilon u_\phi = -\gamma\frac{\partial\varphi}{\partial r} + Ek\left[\nabla^2 u_r - \frac{\gamma^2}{r^2}u_r\right], \tag{2.2}$$

$$\mathrm{D}u_z = -\frac{\partial\varphi}{\partial z} + Ek[\nabla^2 u_z], \tag{2.3}$$

$$\gamma\left(\frac{\partial u_r}{\partial r} + \frac{u_r}{r}\right) + \frac{\partial u_z}{\partial z} = 0, \tag{2.4}$$

where

$$\mathrm{D} = \frac{\partial}{\partial t} + Ro\left[\gamma u_r\frac{\partial}{\partial r} + u_z\frac{\partial}{\partial z}\right],$$

$$\nabla^2 = \gamma^2\left(\frac{\partial^2}{\partial r^2} + \frac{1}{r}\frac{\partial}{\partial r}\right) + \frac{\partial^2}{\partial z^2},$$

$\gamma = b/h$ is the aspect ratio; $Ro = U/b\Omega$ is the Rossby number; $Ek = \nu/b^2\Omega$ is the Ekman number; $\epsilon = 1$ if the rotation is counterclockwise; and $\epsilon = -1$ if the rotation is clockwise.

The choice of scales is by no means unique. Hence there is a proliferation of definitions of dimensionless groups dealing with Dean problem (see Van Dyke 1978). Our choice is inspired by the work of Khesghi & Scriven (1985). An alternative choice that leads to a Reynolds number and a rotation number is also used frequently. Such alternative definitions are clearly related. For example the Reynolds number defined as $Re = bU/\nu$ is related to Rossby and Ekman numbers by $Re = Ro/Ek$, while the rotation number defined as $R_\Omega = b\Omega/U$ is the inverse of Rossby number, i.e. $R_\Omega = 1/Ro$. In the context of the loose-coiling approximation the Dean's parameter lends itself as the natural choice as used by Daskopoulos & Lenhoff (1990). More than a particular choice of scales, it is important to understand the physical interpretation. In our case the Ekman number represents the ratio of viscous to Coriolis force and is held constant at $Ek = 0.01$. The Rossby number represents the ratio of inertial to Coriolis force. As the rotational speed Ω is increased, rotational effects are increased and this corresponds to the *low* Rossby number limit. At higher Rossby numbers, the inertial (including centrifugal terms) effects dominate the solution and flow structures.

We satisfy the continuity equation by introducing the stream function ψ such that

$$u_r = \frac{\gamma}{r}\frac{\partial\psi}{\partial z},\quad u_z = -\frac{\gamma^2}{r}\frac{\partial\psi}{\partial r}. \tag{2.5}$$

Taking the curl of the momentum equations eliminates the potential φ and yields the vorticity transport equation having the streamwise component

$$\mathrm{D}\omega_\phi - Ro\frac{\gamma}{r}u_r\omega_\phi + 2\gamma Ro\frac{u_\phi}{r}\frac{\partial u_\phi}{\partial z} - 2\epsilon\frac{\partial u_\phi}{\partial z} = Ek\left(\nabla^2\omega_\phi - \frac{\gamma^2}{r^2}\omega_\phi\right), \tag{2.6}$$

where ω_ϕ is the streamwise component of the vorticity. The third term in equation (2.6), $(u_\phi/r)\partial u_\phi/\partial z$, is the source term for generating streamwise vorticity by centrifugal force and the fourth term, $\partial u_\phi/\partial z$ is the source term representing the Coriolis

force. Both of them depend on the gradient of the streamwise velocity with respect to the spanwise direction, which is always non-zero owing to the presence of wall boundaries in the spanwise direction. Thus a secondary flow is always present for any non-zero forcing. In the idealized case of infinite extent in the spanwise direction, the basic flow will be one-dimensional and two-dimensional solutions emerge at supercritical bifurcations. In the present case, however, the basic flow is itself two-dimensional with two counter-rotating streamwise vortices. It is also clear that when $\epsilon = -1$ (the co-rotating case), the effects of centrifugal and Coriolis force are additive, but $\epsilon = +1$ results in the two forces opposing each other and a reversal in secondary flow direction becomes possible.

The streamwise vorticity is related to the stream function ψ by

$$\omega_\phi = \gamma \frac{\partial u_z}{\partial r} - \frac{\partial u_r}{\partial z} = -\frac{\gamma}{r} \nabla_2^2 \psi\,; \quad \nabla_2^2 = \gamma^2 \left(\frac{\partial^2}{\partial r^2} - \frac{1}{r} \frac{\partial}{\partial r} \right) + \frac{\partial^2}{\partial z^2}. \tag{2.7}$$

If (2.5) and (2.7) are substituted into (2.6), we obtain the streamwise vorticity equation in stream-function form

$$\frac{\partial}{\partial t} \left(\frac{\gamma}{r} \nabla_2^2 \psi \right) + Ro \left[\frac{\gamma^2}{r} \frac{\partial \psi}{\partial z} \frac{\partial}{\partial r} \left(\frac{\gamma}{r} \nabla_2^2 \psi \right) - \frac{\gamma^2}{r} \frac{\partial \psi}{\partial r} \frac{\partial}{\partial z} \left(\frac{\gamma}{r} \nabla_2^2 \psi \right) - \frac{\gamma^2}{r^2} \frac{\partial \psi}{\partial z} \left(\frac{\gamma}{r} \nabla_2^2 \psi \right) \right]$$
$$- 2\gamma\, Ro \frac{u_\phi}{r} \frac{\partial u_\phi}{\partial z} + 2\epsilon \frac{\partial u_\phi}{\partial z} = Ek \left[\nabla^2 \left(\frac{\gamma}{r} \nabla_2^2 \psi \right) - \frac{\gamma}{r} \left(\frac{\gamma}{r} \nabla_2^2 \psi \right) \right], \tag{2.8}$$

and the streamwise momentum equation can be written as

$$\frac{\partial}{\partial t} (u_\phi) + Ro \left[\frac{\gamma^2}{r} \frac{\partial \psi}{\partial z} \frac{\partial u_\phi}{\partial r} - \frac{\gamma^2}{r} \frac{\partial \psi}{\partial r} \frac{\partial u_\phi}{\partial z} + \frac{\gamma^2}{r^2} \frac{\partial \psi}{\partial z} u_\phi \right] - 2\epsilon \frac{\gamma}{r} \frac{\partial \psi}{\partial z}$$
$$= \frac{\gamma}{r} + Ek \left[\nabla^2 u_\phi - \frac{\gamma^2}{r^2} u_\phi \right]. \tag{2.9}$$

Our task amounts to finding the equilibrium solutions of (2.8) and (2.9) subject to the no-slip and impermeability conditions at the walls of the duct:

$$\psi = \frac{\partial \psi}{\partial r} = 0 \text{ at } r = \beta_i = \frac{\eta}{1-\eta} \text{ and } r = \beta_o = \frac{1}{1-\eta}, \tag{2.10}$$

$$\psi = \frac{\partial \psi}{\partial z} = 0 \text{ at } z = \pm \frac{1}{2}, \tag{2.11}$$

where $\eta = r_i/r_o$ is a measure of the curvature, and β_i and β_o are the dimensionless inner and outer radii of the duct respectively. Observe that in (2.8) the Rossby number multiplies the centrifugal term $2\gamma(u_\phi/r)\partial u_\phi/\partial z$, while the Coriolis term $2\epsilon\partial u_\phi/\partial z$ is of order unity. Thus, as Ro is increased curvature effects will dominate over rotational ones.

3. Numerical algorithms

3.1. *Spectral approximation*

We approximate the stream function ψ and the streamwise velocity u_ϕ by the Chebyshev expansions

$$\psi = \sum_{m=0}^{N_r-1} \sum_{n=0}^{N_z-1} C_{mn}^{\psi} R_m^{\psi}(\tilde{r})\, Z_n^{\psi}(\tilde{z}), \tag{3.1}$$

$$u_\phi = \sum_{m=0}^{N_r-1} \sum_{n=0}^{N_z-1} C^u_{mn} R^u_m(\tilde{r}) Z^u_n(\tilde{z}), \tag{3.2}$$

where

$$\tilde{r} = 2r - \frac{1+\eta}{1-\eta}, \quad \tilde{z} = 2z$$

are algebraic mappings that transform the cross-section of the duct into the domain of Chebyshev polynomials,[-1,1]; R^ψ_m, R^u_m, Z^ψ_n, and Z^u_n are linear combinations of Chebyshev polynomials, chosen to satisfy the no-slip and impermeability conditions at the walls:

$$R^u_l(\tilde{x}) = Z^u_l(\tilde{x}) = T_{l+2}(\tilde{x}) - T_l(\tilde{x}), \tag{3.3}$$

$$R^\psi_l(\tilde{x}) = Z^\psi_l(\tilde{x}) = (l+1)\,T_{l+4}(\tilde{x}) - 2\,(l+2)\,T_{l+2}(\tilde{x}) + (l+3)\,T_l(\tilde{x}), \tag{3.4}$$

for $l = 0, 1, 2, ...$, and $\tilde{x}$ in [-1,1]. A system of nonlinear algebraic equations for the coefficients C^ψ_{mn} and C^u_{mn} is obtained when the Chebyshev expansions of ψ and u_ϕ are substituted into the streamwise vorticity and momentum equations and the resulting equations are satisfied at the Gauss points

$$(\tilde{r}_j, \tilde{z}_k) = \left(\cos\frac{(2j+1)\pi}{2N_r}, \cos\frac{(2k+1)\pi}{N_z}\right) \tag{3.5}$$

for $j = 0, 1, ..., N_r - 1$, $k = 0, 1, ..., N_z - 1$. We write this system symbolically as

$$\boldsymbol{f}(\boldsymbol{C}; \boldsymbol{\lambda}) = 0, \tag{3.6}$$

where $\boldsymbol{C}$ is a vector of size $N = 2N_rN_z$ whose entries are the coefficients C^ψ_{mn} and C^u_{mn}, $\boldsymbol{f}$ is a vector-valued function also of size N that contains the discrete form of the vorticity and momentum equations, and $\boldsymbol{\lambda} = (\gamma, Ro, Ek, \eta)$ is a vector in parameter space. Our task is to solve the system of nonlinear (3.6) as a function of the components of λ. Once the coefficients are found, the flow variables are obtained from (3.1) and (3.2).

3.2. *Continuation schemes*

Based on previous studies (Winters 1987; Nandakumar *et al.* 1991) we expect the flow structure to begin with two counter-rotating streamwise-oriented vortices that bifurcate into more complicated flow structures through several limit or symmetry-breaking points as the Rossby number increases. In the case of curved ducts, the cellular structure is due primarily to curvature effects and in the case of rotating ducts it is due to Coriolis effects. In our case both effects compete with each other, and depending on the curvature and the direction of rotation, four-cell or other structures are possible. Therefore, it is wise to begin the solution at $Ro = 0$ and a large radius of curvature (i.e. $\eta \to 1$), since the equations tend to be linear in that limit. The equations are solved using the Newton method and a zero initial guess. A correction to the estimated solution is found through Newton–Raphson iteration

$$\delta\boldsymbol{C} = J^{-1}\boldsymbol{f} \tag{3.7}$$

where J is the Jacobian of system (3.6). Once a converged solution is obtained, Euler–Newton continuation is used to continue on any chosen parameter, say α, a component of the vector λ. This entails developing a good initial guess for the solution at $\alpha + \Delta\alpha$ from the known solution at α using

$$\boldsymbol{C}(\alpha + \Delta\alpha) = \boldsymbol{C}(\alpha) + \frac{\partial \boldsymbol{C}}{\partial \alpha}\Delta\alpha, \tag{3.8}$$

where $\partial \boldsymbol{C}/\partial\alpha$ is found from differentiating (3.6) with respect to α:

$$J\frac{\partial \boldsymbol{C}}{\partial\alpha} = -\frac{\partial \boldsymbol{f}}{\partial\alpha}. \tag{3.9}$$

This requires only one back substitution since J is already factored during the previous Newton iteration. When this method fails to converge, a nearby singularity is indicated and we switch to the arclength continuation scheme. This entails reparametrizing the problem in terms of arclength, s,

$$\boldsymbol{f}(\boldsymbol{C}(s), \alpha(s)) = 0 \tag{3.10}$$

and introducing an additional constraint which is a measure of the arclength defined by

$$\sum_{j=1}^{N}\left(\frac{\mathrm{d}c_j}{\mathrm{d}s}\right)^2 + \left(\frac{\mathrm{d}\alpha}{\mathrm{d}s}\right)^2 = 1. \tag{3.11}$$

Differentiating (3.10) with respect to s provides

$$\sum_{k=1}^{N}\frac{\partial f_j}{\partial c_k}\frac{\mathrm{d}c_k}{\mathrm{d}s} = -\frac{\partial f_j}{\partial\alpha}\frac{\mathrm{d}\alpha}{\mathrm{d}s}. \tag{3.12}$$

Equations (3.11) and (3.12) are solved for $\mathrm{d}c_j/\mathrm{d}s$ and $\mathrm{d}\alpha/\mathrm{d}s$ and represent a regular system. Once $\mathrm{d}c_j/\mathrm{d}s$ and $\mathrm{d}\alpha/\mathrm{d}s$ are found at a particular s, the Euler method is used predict the solution at $s+\Delta s$:

$$c_j(s+\Delta s) = c_j(s) + \frac{\mathrm{d}c_j}{\mathrm{d}s}\Delta s, \tag{3.13}$$

$$\alpha(s+\Delta s) = \alpha(s) + \frac{\mathrm{d}\alpha}{\mathrm{d}s}\Delta s. \tag{3.14}$$

3.3. *Calculation of singular points*

Quadratic limit points on the solution path $C(\alpha)$ are determined using the extended system formulations of Moore & Spence (1980) and Spence & Werner (1982):

$$\boldsymbol{f}(\boldsymbol{C},\alpha) = 0, \qquad \boldsymbol{f}_{\boldsymbol{C}}(\boldsymbol{C},\alpha)\boldsymbol{v} = 0, \qquad m(\boldsymbol{v}) = 1, \tag{3.15}$$

where $\boldsymbol{v}$ is the right null vector and the constraint $m(\boldsymbol{v}) = 1$ enforces the null vector to be non-trivial. The system of equations (3.15) is known to be regular at the limit point and is solved by a Newton scheme for $(\boldsymbol{C}, \boldsymbol{v}, \alpha)$.

Symmetry-breaking bifurcation points, which lie on the path of symmetric solutions and spawn asymmetric solution branches, are determined by a method proposed by Werner & Spence (1984) which uses the same extended system as (3.15), with the restriction that $\boldsymbol{C} \in X_s, \boldsymbol{v} \in X_a$ where X_s and X_u are the symmetric and antisymmetric subspaces, respectively.

The bifurcation diagrams are illustrated with the dimensionless flow rate, Q, as the state variable, which is calculated from

$$Q = \int_{-0.5}^{+0.5}\int_{\beta_i}^{\beta_o} u_\phi \,\mathrm{d}r\,\mathrm{d}z = \frac{1}{4}\sum_{m=0}^{N_r-1}\sum_{n=0}^{N_z-1} C_{mn}^{u}\int_{-1}^{+1}\int_{-1}^{+1} R_m^u(\tilde{r})\,Z_n^u(\tilde{z})\mathrm{d}\tilde{r}\,\mathrm{d}\tilde{z}.$$

In order to reveal both branches of asymmetric solutions either the stream function or the streamwise velocity on a point away from the line of symmetry is chosen as the state variable.

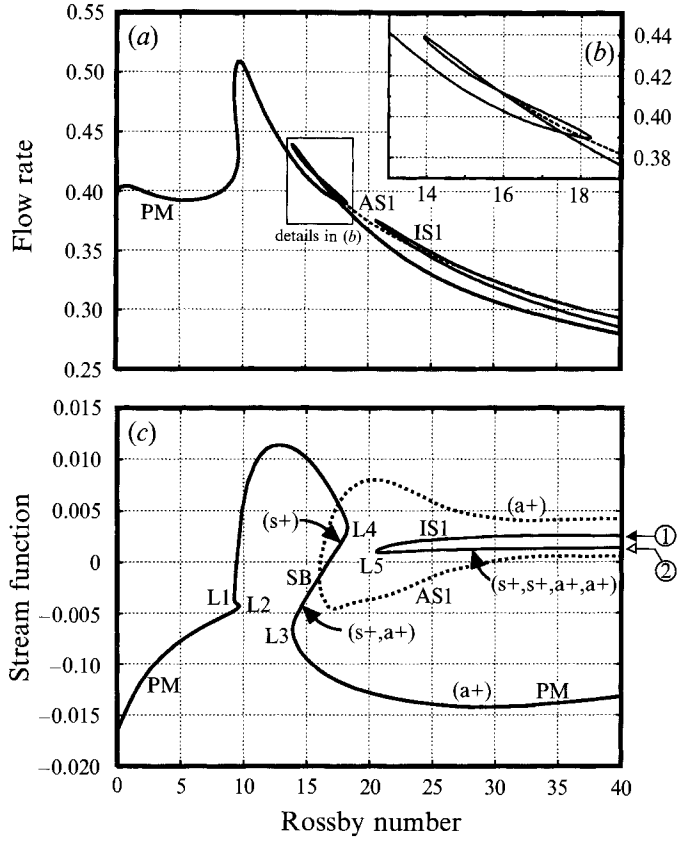

FIGURE 2. State diagrams for the flow through curved, counter-rotating ducts of square cross-section at $Ek = 0.01$ and $\eta = 0.85$. (*a*) Dimensionless flow rate vs. Rossby number, (*b*) detailed view of (*a*), (*c*) stream function at $\tilde{r} = 0.25$, $z = 0.05$ vs. Rossby number.

4. Discussion of results

As recognized first by Itō & Motai (1974), curvature induces a centrifugal force always pointing radially outwards, while system rotation can cause the Coriolis force to be pointing either radially outwards (co-rotation) or radially inwards (counter-rotation). When the effects of system rotation (Coriolis force) oppose those due to curvature (centrifugal force), one can intuitively expect a series of complex flow mutations and secondary flow reversals as a dynamic parameter is gradually varied in parameter space. When the centrifugal and Coriolis effects aid each other, the secondary flow strength is merely intensified. Hence the counter-rotating case is examined first.

We examine in detail the changes in both the *solution structure* and *flow structure* as Rossby number and curvature ratio are varied. By solution structure we mean the number of solution branches and changes in their connectivity and stability. By flow structure we mean the secondary flow pattern, which is characterized by the number of cells and their sense of circulation.

4.1. *Counter-rotation, $\epsilon = 1$*

The scaling of variables has been chosen to correspond to those used by Khesgi & Scriven (1985) and Nandakumar *et al.* (1991). Continuing the focus established

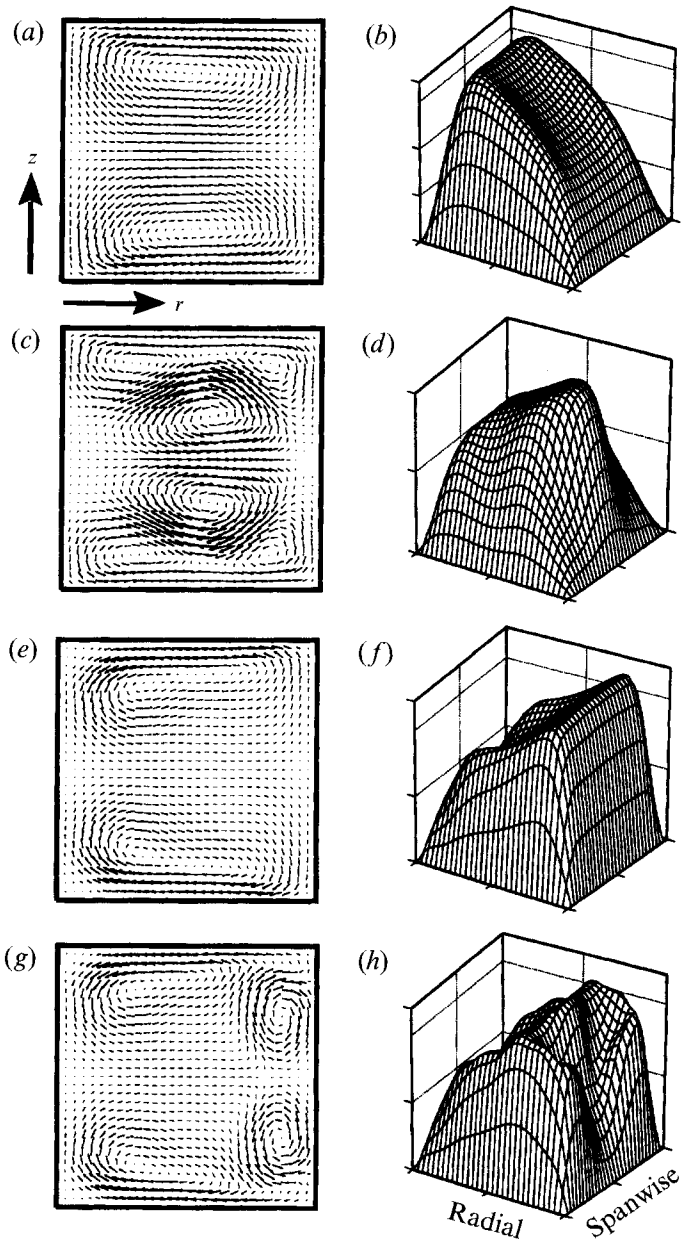

FIGURE 3. Vector plots of secondary flow and perspective plots of streamwise velocity for flow through a curved, counter-rotating duct of square cross section at $Ek = 0.01$, $\eta = 0.85$. (a, b) on the branch PM at $Ro = 5$, (c, d) on the branch PM at $Ro = 10$, (e, f) on the branch IS1 at $Ro = 40$ and point 1, (g, h) on the branch IS1 at $Ro = 40$ and point 2.

in these two studies, the Ekman number is fixed at 0.01 and a square cross-section ($\gamma = 1$) is considered. The computed state diagram for a curvature ratio of $\eta = 0.85$ is shown in figure 2(*a,b*) using flow rate and the stream function at (0.25, 0.05). In the case of rotating straight ducts, all previous work indicates that the flow rate decreases with increasing Ro due to increased resistance caused by secondary flow. Furthermore Nandakumar *et al.* (1991) have computed that up to five solutions can

Point	16 × 16	18 × 18	19 × 19	20 × 20
L1	9.254174	9.254234	9.254054	9.254163
L2	9.639705	9.639561	9.639529	9.639533
L3	13.924666	13.915435	13.911510	13.912308
L4	18.255297	18.251884	18.253340	18.252435
SB1	15.969090	16.007463	15.995551	15.998275
L5	20.564729	20.566255	20.570662	20.569903

TABLE 1. Limit points and symmetry-breaking points for flow through a curved, counter-rotating ($\epsilon = 1$) duct at $\gamma = 1, \eta = 0.85$ and $Ek = 0.01$

Ro	Branch	Symmetric modes	Antisymmetric modes
9.5	PM before L2	Stable	Stable
	PM between L1-L2	0.095538	No addition
	PM between L1-L4	Stable	Stable
15	PM between L1-L4	Stable	Stable
	PM between SB-L3	0.52057	0.56061
	PM beyond L3	Stable	0.42478
17	PM between L1-L4	Stable	Stable
	PM between SB-L4	0.62105	$0.13742 \pm 0.4080\,i$
	PM beyond L3	Stable	0.27998
	AS1	-	$0.56175 \pm 0.3007\,i$
40	IS1 (point 1)	Stable	Stable
	IS1 (point 2)	5.1768	4.0464
		$0.13869 \pm -5.0123\,i$	1.9493

TABLE 2. Calculated eigenvalues for curved counter-rotating ($\epsilon = 1$) duct at $\gamma = 1, \eta = 0.85$ and $Ek = 0.01$

exist at $Ro = 5$, all of them being unstable. Figure 2(*a*), however, shows a unique stable two-cell solution for *Ro* as high as 9.25 when curvature is present. Furthermore, there is a sharp increase in flow rate near a Rossby number of 9.0.

The physical mechanisms responsible for such behaviour are easily understood once we recognize that a finite curvature has the tendency to induce a secondary flow directed radially outward in the middle of the channel while a system rotation has a tendency to induce secondary flow in the radially inward direction. At low *Ro*, the rotational effect dominates the flow, which must be weakened by the increasing magnitude of centrifugal force with increasing *Ro*. Thus the net secondary flow is actually weakened over a certain range of *Ro*, resulting in a net increase in the streamwise flow rate, as well as a delay in the flow mutations.

Vector plots of secondary flow and perspective plots of streamwise velocity are shown in figure 3(*a–h*). These illustrate the changes in flow structure with increasing Rossby number. At low Rossby numbers ($Ro = 5$ in figure 3*a,b*) the secondary flow has a two-cell structure. The secondary flow is pointed radially inwards (Coriolis-force-dominated flow) at $z = 0$ as seen from the vector plot, as well as from the indirect evidence of shift in the maximum of streamwise velocity towards the inner

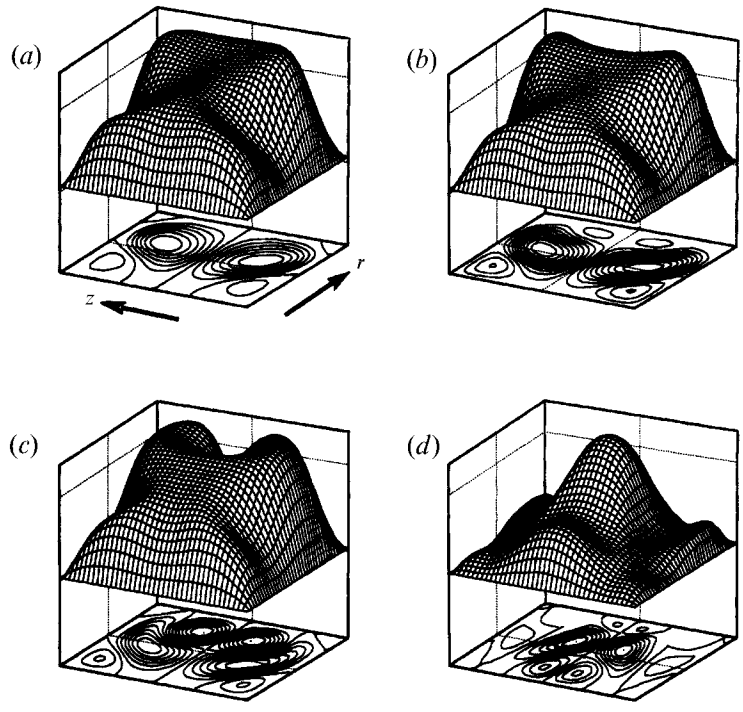

FIGURE 4. Perspective plots of streamwise velocity and contour plots of stream function for the flow through curved, counter-rotating ducts of square cross section at $Ek = 0.01$, $\eta = 0.85$: (*a*) on the branch PM before $L4$ at $Ro = 17$, (*b*) on the branch PM between $L4$ and $L3$ at $Ro = 17$, (*c*) on the branch PM after $L3$ at $Ro = 17$, (*d*) the asymmetric solution on the branch $AS1$ at $Ro = 17$.

radial wall. At $Ro = 10$, in figure 3(*c,d*), the secondary flow reversal has begun with the formation of two additional strong cells in the middle of the duct with a radially outward flow in the middle of the duct and a corresponding shift in the maximum streamwise velocity towards the outer wall. In this range of Rossby number, the centrifugal force begins to dominate the rotational effect. Figure 3(*e,f*) shows the flow pattern where the centrifugal force dominates the flow field at $Ro = 40$ and the secondary flow direction is completely reversed. This is at the point labelled 1 on branch IS1 in figure 2(*c*). As will be shown later, this part of branch IS1 actually becomes connected to the primary branch PM through a transcritical point and hence it inherits the stability and flow structure of branch PM. On the other side of branch IS1 (labelled 2) additional cells are formed near the outer wall as seen in figure 3(*g,h*). Except for the flow structure shown in figure 3(*c,d*), all of the other flow structures are similar to previously determined patterns in the presence of curvature or rotation alone.

At sufficiently large Ro ($Ro > 10$ in figure 2*a*), the centrifugal force is established as the dominant mechanism and the mean flow continues to *decrease* with increasing Ro and further flow bifurcations take place. The solution structure is, however, different from that computed in Nandakumar *et al.* (1991) for a straight rotating duct, or by Winters (1987) for a stationary curved duct, thus establishing that the system rotation has a strong influence on the solution structure. All of the computed limit and symmetry-breaking points are given in table 1. This table also provides a measure of the adequacy of the spectral resolution. The lower limit points are accurate up to

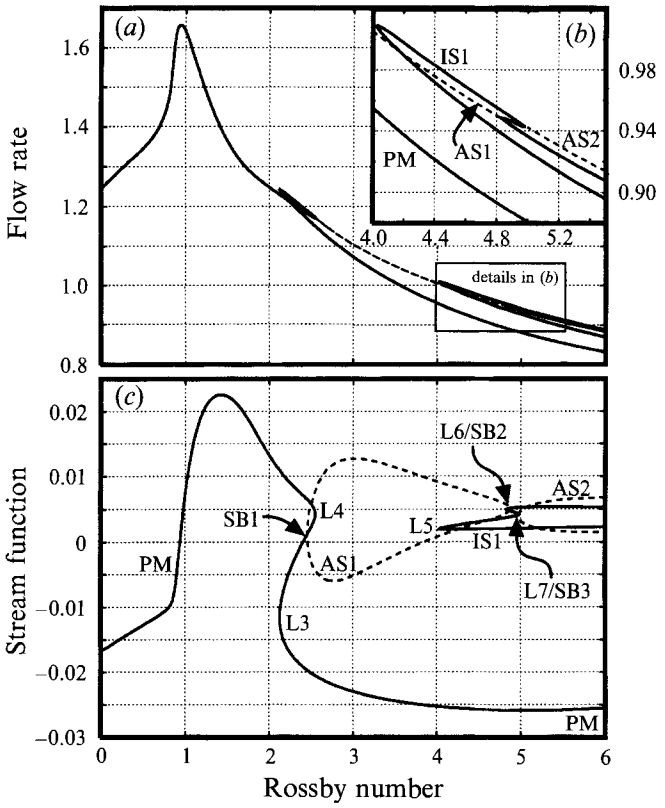

FIGURE 5. State diagrams for the flow through curved, counter-rotating ducts of square cross section at $Ek = 0.01$ and $\eta = 0.60$. (*a*) Dimensionless flow rate vs. Rossby number, (*b*) detailed view of (*a*), (*c*) stream function at $\bar{r} = 0.25$, $z = 0.05$ vs. Rossby number.

five significant digits while the higher ones have three-significant-digit accuracy. Most of the results were obtained at a resolution of 16×16.

The limit points are labelled in increasing numerical order in figure 2(*c*). Limit points L1 and L2 correspond to the switch in the dominant mechanism from Coriolis to centrifugal force. The stability of these branches was determined by computing the complete spectrum of eigenvalues of the discrete problem at selected values of *Ro*. Spectral methods are notorious for introducing spurious modes. Fortunately they are also easy to detect using a few markers. Firstly such spurious modes are an order of magnitude larger in value. They are also extremely sensitive to spectral refinement. Using these markers along with the expected change in stability at singular points we can piece together a reasonably consistent stability picture. The uncertainties in this scenario can arise due to undetected singular points, particularly Hopf points or bifurcation of three-dimensional solutions, both of which are not investigated here.

Results of the stability calculations are summarized in table 2 and are also marked in figure 2(*c*). Here the notation is as follows: each (s+) refers to one positive, symmetric mode and each (a+) refers to one positive antisymmetric mode. The primary branch PM starting at the origin $Ro = 0$ remains stable until the limit point L2. The intermediate branch between L1 and L2 has developed one unstable mode and part of the primary branch between L1 and L4 remains stable to both symmetric and asymmetric perturbations. Since the symmetry-breaking point SB is

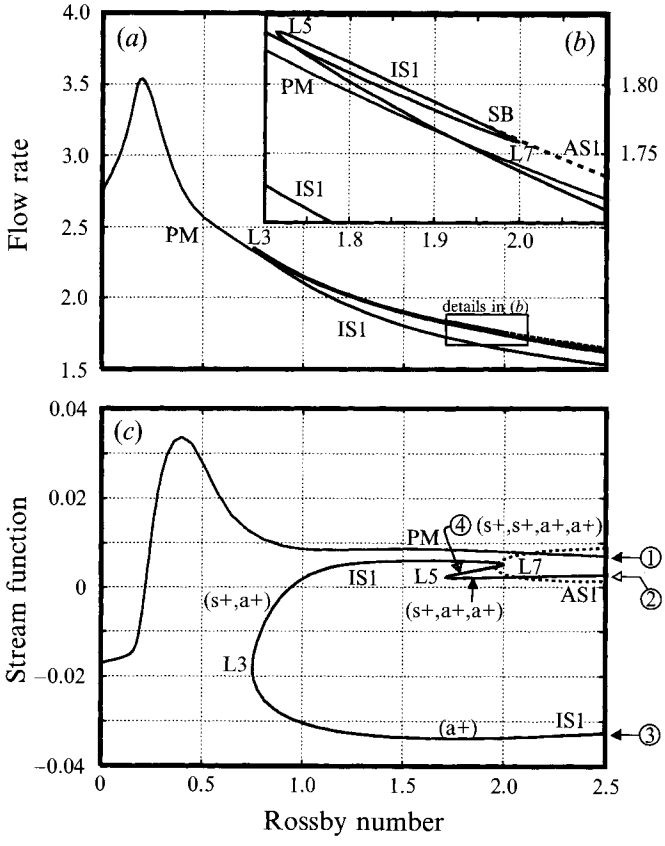

FIGURE 6. State diagrams for the flow through curved, counter-rotating ducts of square cross section at $Ek = 0.01$ and $\eta = 0.30$. (*a*) Dimensionless flow rate vs. Rossby number, (*b*) detailed view of (*a*), (*c*) stream function at $\bar{r} = 0.25$, $z = 0.05$ vs. Rossby number.

around $Ro = 16$, stability of PM between L3 and L4 is determined by calculating eigenvalues on either side of SB, viz. at $Ro = 15, 17$. Between L4 and SB there appears one unstable symmetric mode which is consistent with crossing over one limit point. There is also a pair of complex eigenvalues with a positive real part. This anomaly might be indicative of the presence of a Hopf point in this neighbourhood. Between SB and L3, a symmetric and an antisymmetric unstable mode are found and this is consistent with crossing over a symmetry-breaking point. Turning around L3, the unstable symmetric mode disappears, leaving one unstable asymmetric mode. Thus, part of the branch PM past L3 is stable with respect to symmetric perturbations and unstable to asymmetric perturbations, a result which is similar to that found in the Dean and rotating straight duct problems. The upper part of the branch IS1 in figure 2(*c*) is found to be stable, while the lower part has several unstable modes.

Note that between SB and L4, there are five different solutions, two of which are asymmetric. Typical flow patterns of these multiple solutions are shown in figure 4(*a–d*) at $Ro = 17$. Since the pair of asymmetric solutions are mirror images of each other, the flow pattern of only one is shown in figure 4(*d*). The degree of asymmetry is seen to be very small as is typical in this class of flows. The small vortices found near the corner of the inner wall in figure 4(*a*) are remnants the Coriolis mechanism. Since the centrifugal force begins to dominate at these Rossby numbers, the unstable

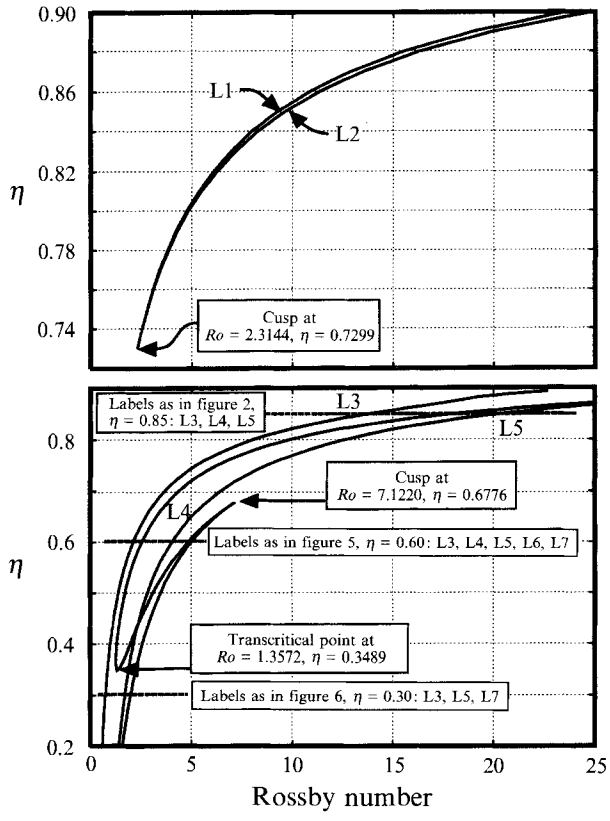

FIGURE 7. Variation of limit points with curvature ratio and Rossby number for the flow through curved and counter-rotating ducts of square cross section at $Ek = 0.01$.

flow domain is near the outer wall, where two additional cells are seen to be born in figure 4(*b*) and grow in size and strength in 4(*c*).

4.2. *Effect of curvature with counter-rotation*

In order to determine how the solution structure changes with changing curvature ratio, two additional bifurcation diagrams were computed at $\eta = 0.6$ and 0.3. They are shown in figures 5 and 6 respectively. Note that there are significant structural differences between the bifurcation diagrams at $\eta = 0.85, 0.6$ and 0.3. As η is decreased, the bifurcations take place at lower values of Ro. A comparison of the centrifugal and Coriolis source terms in (2.6) (viz. $\gamma\, Ro\,(u_\phi/r)\partial u_\phi/\partial z$, and $\partial u_\phi/\partial z$) together with the definition of $Ro = U/b\Omega$ is helpful in interpreting some of the trends displayed in figures 2,5 and 6. Since decreasing η implies tighter coils (i.e. smaller radius of curvature) the two terms identified above balance each other at lower values of Ro. Clearly flow mutations and secondary flow reversals begin to occur when these two terms cancel each other. Such cancellations occur at lower Ro with decreasing η due to the appearance of (Ro/r) in the centrifugal force term, i.e. the centrifugal force term begins to dominate at lower values of Ro as η is decreased.

In the absence of system rotation, Winters (1987) has determined that decreasing the radius of curvature tends to delay flow transitions with respect to Dean number, i.e. the singular points move to higher values of the Dean number. But there are no structural changes in the solution, implying that there are no higher-order singularities

Point	16×16
L3	0.7526400
L5	1.712792
L7	1.998927
SB	1.960775

TABLE 3. Limit points and symmetry-breaking points for flow through a curved counter-rotating ($\epsilon = 1$) duct at $\gamma = 1, \eta = 0.30$ and $Ek = 0.01$

No.	*Ro*	Branch	Symmetric modes	Antisymmetric modes
1	2.5	PM	Stable	Stable
2	2.5	IS1	3.59608	2.9669687 0.87443573
3	2.5	IS1	stable	0.84616624
4	1.84	IS1 $\in \{L2, L3\}$	1.77979 0.3873218	1.73691789 0.29354811

TABLE 4. Calculated eigenvalues for curved counter-rotating ($\epsilon = 1$) duct at $\gamma = 1, \eta = 0.30$ and $Ek = 0.01$

on the fold curves of curvature *vs.* Dean number. In the present problem, however, there are significant structural changes as curvature is varied. Such changes are tracked by following the variation of all the limit points found in figures 2,5 and 6 using (3.15). The resulting fold curves are shown in figure 7. The limit points L3 and L5 in figure 2 remain robust over the entire range of $\eta \in [0.2, 0.85]$. The limit points L1 and L2 disappear through a cusp at ($Ro = 2.3144, \eta = 0.7299$). Below this value of η the secondary flow reversal still takes place, but it is a smooth process as seen in figures 5 and 6. The signature for flow reversal in these figures is the net increase in streamwise flow rate and change in sign of the stream function.

The other major structural change concerns how the primary branch PM in figure 2 becomes connected to IS1. This takes place with the birth of two additional limit points L6 and L7 on the upper part of branch IS1 in figure 5. The fold curves in figure 7 reveal that L6 and L7 are born at a cusp near ($Ro = 7.1220, \eta = 0.6776$). With continued decrease in η, L6 and L4 merge at a transcritical point near ($Ro = 1.3572, \eta = 0.3489$). In this process the upper part of IS1 in figure 2(*c*) becomes connected to PM and also inherits its stability properties as seen in figure 6. The limit-point values and a summary of eigenvalue calculations at $\eta = 0.3$ are shown in tables 3 and 4, respectively. The locations where the eigenvalues are computed are labelled 1 to 4 in figure 6.

The bifurcation diagram in figure 5(*c*) bears a strong resemblance to that computed by Nandakumar *et al.* (1991) for a rotating straight duct. The asymmetric branch that originates on PM at SB1 (near L4) terminates at SB2 (near L6) which is on the isolated symmetric branch IS1. A second asymmetric branch AS2 originates at SB3 (near L7) on IS1. As in related problems of rotating straight ducts (Nandakumar *et al.* 1991)

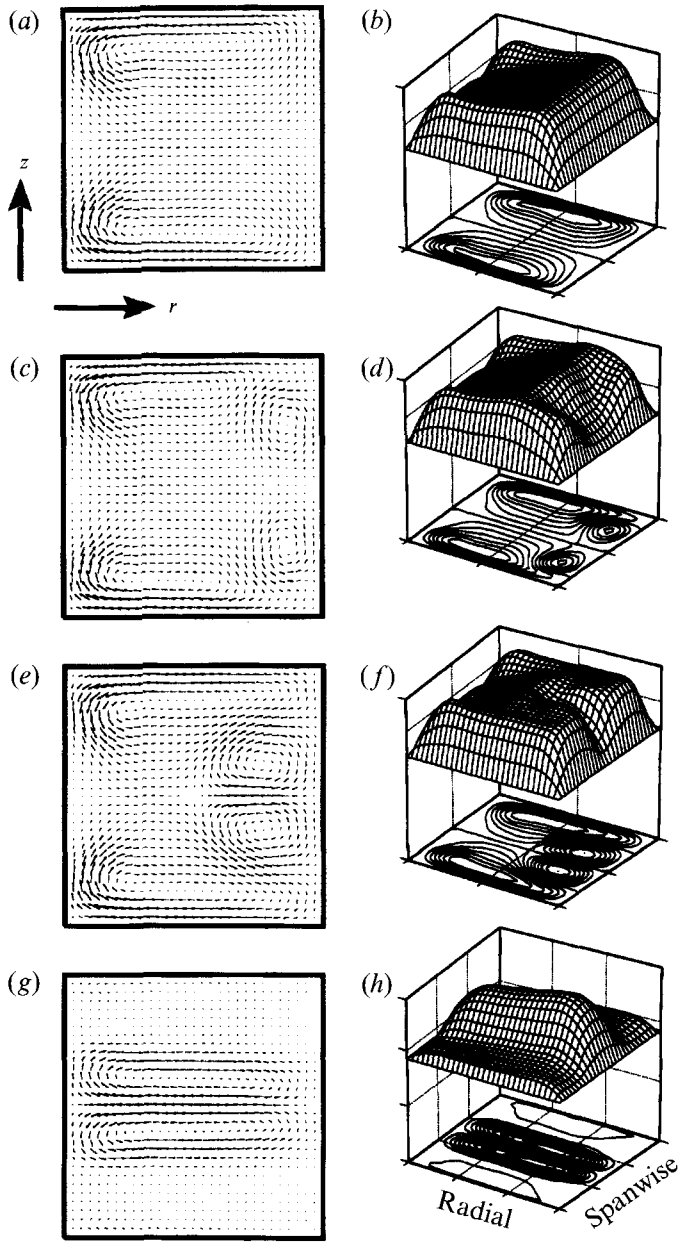

FIGURE 8. Vector plot of secondary flow, and perspective plots of streamwise velocity and contours of stream function for the flow through curved, counter-rotating ducts of square cross-section at $Ek = 0.01$, $\eta = 0.36$ and $Ro = 2.5$. (a, b) the first solution on the curve PM, (c, d) the second solution on the curve $IS1$ (point 2 in figure 6c), (e, f) the third solution on the curve $IS1$ (point 3 in figure 6c), (g, h) the asymmetric solution on the branch $AS1$.

and heated straight ducts (Nandakumar & Weinitschke 1991), the symmetry-breaking points and limit points are always closely spaced. Any geometrical perturbation that breaks the symmetry, such as a change in the orientation (tilt) of the duct with respect to the z-axis will unfold the symmetry-breaking points into limit points which merge typically with the nearby limit point at a cusp.

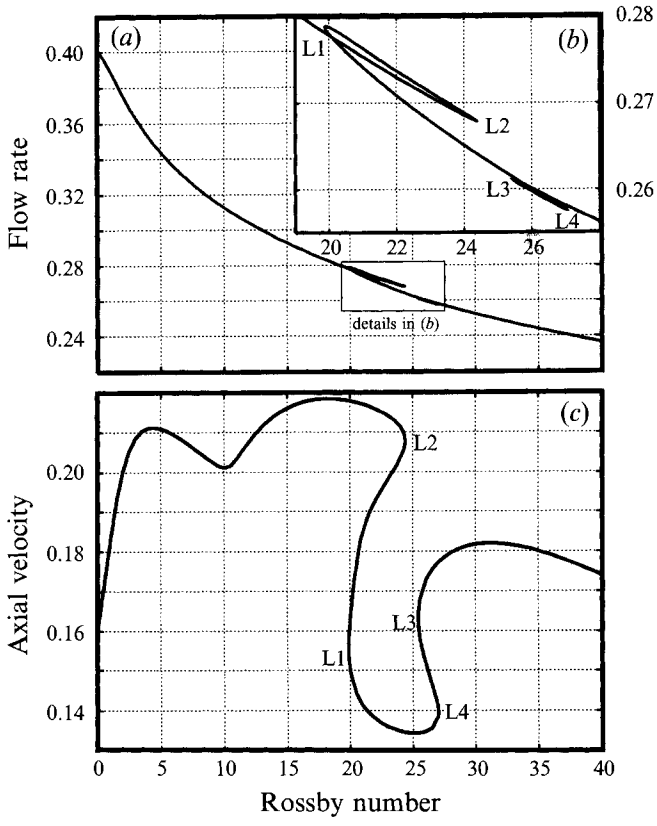

FIGURE 9. State diagrams for the flow through curved, co-rotating ducts of square cross section at $Ek = 0.01$ and $\eta = 0.85$. (*a*) Dimensionless flow rate vs. Rossby number, (*b*) detailed view of (*a*), (*c*) streamwise velocity at $\tilde{r} = 0.45$, $z = 0.25$ vs. Rossby number.

The stability picture on either side of L3 in figures 2(*c*) and 6(*c*) remains the same, with the lower branch having one asymmetric unstable mode and the upper branch having a symmetric and asymmetric unstable mode. The flow profiles of multiple solutions in figure 6(*c*) at $Ro = 2.5$ are shown in figure 8(*a–h*). The primary branch PM has a two-cell flow structure, with the secondary flow at $z = 0$ directed towards the outer wall. The flow profiles at points 2 and 3 on branch IS1 have a four-cell flow structure and are similar to the ones observed earlier by Nandakumar *et al.* (1991). The asymmetric profile shown in figure 8(*g,h*) appears, however, to be quite different with four cells spanning the entire width of the duct and with very strong circulation in the middle of the channel. The flow at $z = 0$ in figure 8(*g*) is seen to be directed towards the inner wall. The degree of asymmetry is also quite small.

4.3. *Co-rotation*, $\epsilon = -1$

In the co-rotating case, secondary flow reversal does not take place, since both the Coriolis and centrifugal forces drive the secondary flow in the same direction. The state diagrams using mean flow rate and streamwise velocity at a point are shown in figure 9(*a–c*) for the case of $\eta = 0.85, Ek = 0.01$. Unlike in the counter-rotating case, and as expected for the present case, the mean flow decreases with increasing Ro since the secondary flow is continuously strengthened with increasing Ro. Four limit points are located on the primary symmetric branch and the limit-point values are

Point	16×16	20×20
L1	19.834579	19.8888
L2	24.444803	24.4085
L3	25.959702	25.4307
L4	27.790847	27.0220

TABLE 5. Limit points for flow through a curved co-rotating ($\epsilon = -1$) duct at $\gamma = 1, \eta = 0.85$ and $Ek = 0.01$

No.	Ro	Branch	Symmetric modes	Antisymmetric modes
1	21.75	PM before L2	Stable	Stable
2	21.75	PM $\in \{L1, L2\}$	1.3518 $0.3002 \pm 1.4108\, i$	1.4326 $0.11054 \pm 1.4530\, i$
3	21.75	PM $\in \{L1, L4\}$	$3.9153 \pm 0.73946\, i$	4.5074 $1.7954 \pm 0.79507\, i$

TABLE 6. Calculated eigenvalues for curved co-rotating ($\epsilon = -1$) duct at $\gamma = 1, \eta = 0.85$ and $Ek = 0.01$

shown in table 5. The stability results are summarized in table 6. The primary branch is found to be stable to both symmetric and asymmetric perturbations until the limit point L2. Continuing on this path, pairs of complex eigenvalues with positive real part are found between (L2,L1) and (L1,L4).

The flow structure is revealed in figure 10(*a–d*), three of which are multiple solutions at $Ro = 21.75$ and the fourth one is shown at $Ro = 40$. The maximum of streamwise velocity is always found near the outer radial wall and no flow reversals are found. Flow mutations with the formation of additional cells near the outer wall still take place as Ro is increased. Note that the regions near the outer wall are unstably stratified.

5. Concluding remarks

Although the problem of flow in curved rotating ducts has been studied previously by Miyazaki (1973), a very rich solution structure, hitherto unknown, has been revealed in the present study. These include asymmetric solution branches that emanate at symmetry-breaking bifurcation points and isolated symmetric solution branches. All of the asymmetric solution branches have been determined to be unstable. It is still not clear whether for rotating curved pipes (Daskopoulos & Lenhoff 1990) similar asymmetric solutions are possible, since symmetry has been imposed in all of the earlier works. The demonstration by Itō & Motai (1974) that secondary flow reversals can take place in rotating curved pipes has been reaffirmed in the present study for rotating curved ducts. This occurs when the effect of system rotation opposes that of curvature. Unlike in the Dean problem (i.e. stationary curved ducts), the solution structure has been found to change significantly with changing radius of curvature.

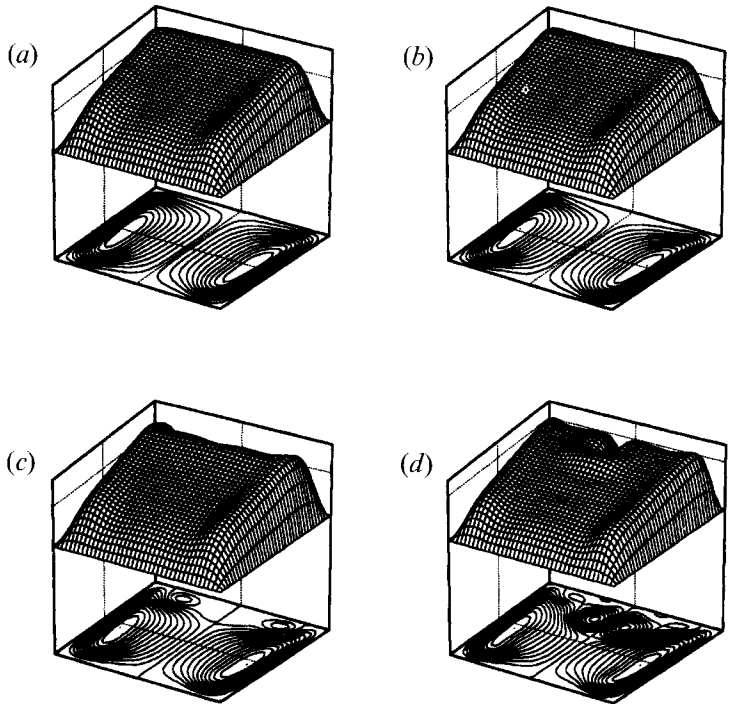

FIGURE 10. Perspective plots of streamwise velocity and contour plots of stream function for the flow through curved, co-rotating ducts of square cross section at $Ek = 0.01$, $\eta = 0.85$. (*a*) The first solution on the curve PM before $L2$ at $Ro = 21.75$, (*b*) the second solution on the curve PM between $L2$ and $L1$ at $Ro = 21.75$, (*c*) the third solution on the curve PM after $L1$ at $Ro = 21.75$, (*d*) the solution on the branch PM at $Ro = 40$.

Continued financial support to KN and WHF from the Natural Sciences and Engineering Research Council of Canada is gratefully acknowledged. The authors are grateful to one of the referees for valuable comments which helped in clarifying the presentation.

REFERENCES

ALFREDSSON, P. A. & PERSSON, H. 1989 Instabilities in channel flow with system rotation. *J. Fluid Mech.* **202**, 543–557.

BARA, B., NANDAKUMAR, K. & MASLIYAH, J. H. 1992 An experimental and numerical study of the Dean problem: flow development towards two-dimensional multiple solutions. *J. Fluid Mech.* **244**, 339–376.

BARUA, S. N. 1954 On secondary flow in stationary curved pipes. *Proc. R. Soc. Lond.* A **227**, 133–139.

BERGER, S. A., TALBOT, L. & YAO, L-S. 1983 Flow in curved pipes. *Ann. Rev. Fluid Mech.* **15**, 461–512.

CHENG, K. C. & AKIYAMA, M. 1970 Laminar forced convection heat transfer in curved rectangular channels. *Intl J. Heat Mass Transfer* **13**, 471–490.

CHENG, K. C., NAKAYAMA, J. & AKIYAMA, M. 1979 Effect of finite and infinite aspect ratios on flow patterns in curved rectangular channels. In *Flow Visualization 1977*. Hemisphere.

DASKOPOULOS, P. & LENHOFF, A. M. 1989 Flow in curved ducts: bifurcation structure for stationary ducts. *J. Fluid Mech.* **203**, 125–148.

DASKOPOULOS, P. & LENHOFF, A. M. 1990 Flow in curved ducts. Part 2. Rotating ducts. *J. Fluid*

Mech. **217**, 575–593.

DEAN, W. R. 1927 Note on the motion of fluid in a curved pipe. *Phil. Mag.* **4**, 208–223.

DENNIS, S. R. C. 1980 Calculation of the steady flow through a curved tube using a new finite difference method. *J. Fluid Mech.* **99**, 449–467.

DENNIS, S. R. C. & RILEY, N. 1982 On the fully developed flow in a curved pipe at large Dean number. *Proc. R. Soc. Lond.* A **434**, 473–478.

DUCK, P. 1983 Flow through rotating straight pipes of a circular cross section. *Phys. Fluids* **26**, 614–618.

DURST, F. & RASZILLIER, H. 1990 Flow in a rotating straight pipe with a view on Coriolis mass flow meters. *Trans. ASME* I *J. Fluids Engng* **112**, 149–154.

EUSTICE, J. 1910 Flow of water in curved pipes. *Proc. R. Soc. Lond.* A **84**, 107–118.

EUSTICE, J. 1911 Experiments on stream-line motion in curved pipes. *Proc. R. Soc. Lond.* A **85**, 119–131.

FINLAY, W. H. 1990 Transition to oscillatory motion in rotating channel flow. *J. Fluid Mech.* **215**, 209–227.

FINLAY, W. H. 1992 Transition to turbulence in a rotating channel. *J. Fluid Mech.* **237**, 73–99.

GHIA, K. N. & SOKHEY, J. S. 1977 Laminar incompressible viscous flow in curved ducts of regular cross-section. *Trans. ASME* I *J. Fluids Engng* **99**, 640–648.

HART, J. E. 1971 Instability and secondary motion in a rotating channel flow. *J. Fluid Mech.* **45**, 341–351.

HILLE, P., VEHRENKAMP, R. & SCHULZ-DUBOIS, E. O. 1985 The development and structure of primary and secondary flow in a curved square duct. *J. Fluid Mech.* **151**, 219–241.

HOCKING, L. M. 1967 Boundary and shear layers in a curved rotating pipe. *J. Math. Phys. Sci.* **1**, 123–136.

HUMPHREY, J. A. C., TAYLOR, A. M. K. & WHITELAW, J. H. 1977 Laminar flow in a square duct of strong curvature. *J. Fluid Mech.* **83**, 509–527.

ITŌ, H. & MOTAI, T. 1974 Secondary flow in a rotating curved pipe. *Rep. Inst. High Speed Mech.* **29**, 33–57.

KHESHGI, H. S. & SCRIVEN, L. E. 1985 Viscous flow through a rotating square channel. *Phys. Fluids* **28**, 2868–2979.

LEZIUS, D. K. & JOHNSTON, J. P. 1976 Roll-cell instabilities in rotating laminar and turbulent channel flows. *J. Fluid Mech.* **77**, 153–175.

LUDWIEG, H. 1951 Die ausgebildete Kanalströmung in einem rotierenden System. *Ingenieur-Archiv* **19**, 296–308.

MANSOUR, K. 1985 Laminar flow through a slowly rotating straight pipe. *J. Fluid Mech.* **150**, 1–21.

MIYAZAKI, H. 1971 Combined free and forced convective heat transfer and fluid flow in a rotating curved circular tube. *Intl J. Heat Mass Transfer* **14**, 1295–1309.

MIYAZAKI, H. 1973 Combined free and forced convective heat transfer and fluid flow in a rotating curved rectangular tube. *Trans. ASME* C: *J. Heat Transfer* **95**, 64–71.

MOORE, G. & SPENCE, A. 1980 The calculation of turning points of non-linear equations. *SIAM J. Numer. Anal.* **17**, 567–576.

NANDAKUMAR, K. & MASLIYAH, J. H. 1986 Swirling flow and heat transfer in coiled and twisted pipes. *Adv. Transport Processes* **4**, 49–112.

NANDAKUMAR, K., RASZILLIER, H. & DURST, F. 1991 Flow through rotating rectangular ducts. *Phys. Fluids* A **3**, 770–781.

NANDAKUMAR, K. & WEINITSCHKE, H. J. 1991 A bifurcation study of mixed convection heat transfer in horizontal ducts. *J. Fluid Mech.* **231**, 157–187.

PIESCHE, M. & FELSH, K.-O. 1980 Experimental investigation of pressure loss in rotating curved rectangular channels. *Arch. Mech.* **32**, 747–756.

RAMSHANKAR, R. & SREENIVASAN, K. R. 1988 A paradox concerning the extended Stokes series solution for the pressure drop in coiled pipes. *Phys. Fluids* **31**, 1339–1347.

RASZILLIER, H. & DURST, F. 1991 Coriolis-effect in mass flow metering. *Arch. Appl. Mech.* **61**, 192–214.

SANKAR, S. R., NANDAKUMAR, K. & MASLIYAH, J. H. 1988 Oscillatory flows in coiled square ducts. *Phys. Fluids* **31**, 1348–1358.

SHANTHINI, W. & NANDAKUMAR, K. 1986 Bifurcation phenomena of generalized newtonian fluids

in curved rectangular ducts. *J. Non-Newtonian Fluid Mech.* **22**, 35–60.

SOH, W. Y. 1988 Developing fluid flow in a curved duct of square cross-section and its fully developed dual solutions. *J. Fluid Mech.* **188**, 337–361.

SPENCE, A. & WERNER, B. 1982 Non-simple turning points and cusps. *IMA J. Numer. Anal.* **2**, 413–427.

SPEZIALE, C. G. 1982 Numerical study of viscous flow in rotating rectangular ducts. *J. Fluid Mech.* **122**, 251–271.

SPEZIALE, C. G. & THANGAM, S. 1983 Numerical study of secondary flows and roll-cell instabilities in rotating channel flow. *J. Fluid Mech.* **130**, 377–395.

SUGIYAMA, S., HAYASHI, T. & YAMAZAKI, K. 1983 Flow characteristics in the curved rectangular channels (visualization of secondary flow). *Bull. JSME* **26**, 964–969.

TAYLOR, A. M. K. P., WHITELAW, J. H. & YIANNESKIS, M. 1982 Curved ducts with strong secondary motion: velocity measurements of developing laminar and turbulent flow. *Trans. ASME* I: *J. Fluids Engng* **104**, 350–359.

VAN DYKE, M. 1978 Extended stokes series: laminar flow through a loosely coiled pipe. *J. Fluid Mech.* **86**, 129–145.

WALKER, J. S. 1975 Steady flow in a rapidly rotating variable area rectangular ducts. *J. Fluid Mech.* **69**, 209–227.

WERNER, B. & SPENCE, A. 1984 The computation of symmetry breaking bifurcation points. *SIAM J. Numer. Anal.* **21**, 388–399.

WINTERS, K. H. 1987 A bifurcation study of laminar flow in a curved tube of rectangular cross-section. *J. Fluid Mech.* **180**, 343–369.

WINTERS, K. H. & BRINDLEY, R. C. G. 1984 *Multiple solutions for laminar flow in helically-coiled tubes. AERE Rep.* 11373. AERE Harwell, UK.

YEE, G., CHILUKURI, R. & HUMPHERY, J. A. C. 1980 Developing flow and heat transfer in strongly curved ducts of rectangular cross section. *Trans. ASME* C: *J. Heat Transfer* **102**, 285–291.